DEVELOPMENT OF METHODS FOR LIDAR SENSING OF AEROSOL ATMOSPHERE

G.G. Matvienko

Institute of Atmospheric Optics,
Siberian Branch of the Russian Academy of Sciences, Tomsk
Received October 27, 1994

Single–frequency methods of laser sensing of aerosol atmosphere are discussed in detail in this paper. Basic data on spatiotemporal variability of natural aerosols are presented and the relation of its variations to the atmospheric turbulence are analyzed. Capabilities of ground–based and airborne lidars are explored in such applications as mapping, the large–scale transport of aerosol pollutants, and the determination of power of local sources of atmospheric emissions. Incoherent methods of sensing altitude profiles of horizontal wind velocity are described. Laser soundings of cloud fields with a spaceborne laser range finder in 1982–1983 are reported, in the context of discussion of aerosol measurements from space.

Aerosol is an important constituent of the atmosphere. It influences in many ways on the radiative field, weather formation, and it is involved in many physical and chemical reactions including those connected with the industrial pollution of atmospheric air. Atmospheric aerosol exhibits marked spatiotemporal variation whose magnitude may serve as an indicator of dynamics of the atmospheric physical state.

Since aerosol is so important, it has been the subject of many studies and has required the development of many modern devices, both for direct and indirect measurements. Among indirect devices, of importance are lidars which implement the methods of remote laser sensing of the atmosphere.[1–3]

Atmospheric aerosol, normally returning strong signals, is easy to investigate by laser sensing facilities, since even low–quality aerosol lidars can operate at large ranges. On the other hand, aerosol is a multiparameter variable, thus seriously complicating the inversion of optical parameters of scattered lidar returns into physical properties of aerosol particles.[1,3,4] As shown in Ref. 4, stable solutions for microphysical parameters of aerosol particles are obtained using multispectral analysis of lidar returns at selected wavelengths. Single–frequency lidars are efficient for determination of the altitude characteristics of the slant visual range, mass concentration (or water content if water–drop aerosol), optical coefficients of scattering (attenuation) by natural and anthropogenic aerosols, and the parameters of motion of aerosol formations.

Laser sensing techniques are intensively developed at the Institute of Atmospheric Optics. Academician V.E. Zuev and colleagues have developed a series of lidars for use in both stationary and field measurements: from those onboard automobile trailer to shipborne, airborne, or even spaceborne lidars, such as Balkan–1.[5] Among those such lidar systems as Elektronika–01, 03, and 06 (Ref. 6) are put into serial production.

The above lidar systems use single–frequency sensing techniques, which are simpler to implement than multifrequency ones, but meet the modern practical demands. The present paper discusses single–frequency lidar methods of studying aerosol atmosphere, being developed currently at the Institute of Atmospheric Optics. Most attention is paid to sensing methods for treating spatiotemporal variations of aerosol fields, mapping of industrial aerosols over cities, evaluation of atmospheric wind and turbulence, as well as the applications to satellite and airborne remote monitoring.

SPATIOTEMPORAL VARIATIONS OF AEROSOL FIELDS

Atmospheric aerosol is in continuous agitation due to atmospheric turbulence, in the presence of random pulsations of velocity, temperature, and other atmospheric admixtures. So, the aerosol itself experiences strong spatiotemporal fluctuations (both in concentration and microstructure). A by–product of such fluctuations are varying lidar returns,[7,8] exhibiting common features with turbulent pulsations (close shapes of structure functions and spectral densities of lidar signals and the observed wind pulsations under the conditions of stable, indifferent, and unstable stratification). In principle, this makes it possible to develop methods of remote measurements of atmospheric turbulence using ordinary incoherent aerosol lidar.

A comprehensive study of fluctuations of natural aerosol fields was undertaken in 1993, in the course of special field experiment.[9] The primary means in that experiment were three ultrasonic meteorological stations[10] and aerosol lidar LOZA–3 (Ref. 11). The thermal situation in the near–ground layer was controlled with a sodar. Measurements were performed within the near–ground atmospheric layer.

Acoustic meteorological stations recorded, at a repetition rate of 10 Hz, local values of three wind velocity components and air temperature. Meteorological stations were located at altitudes of 2, 5, and 10 m, one of which (number 3, at 5–m altitude) was 240 m away from the lidar. The arrangement of experiment is shown in Fig. 1. The lidar path run along in the immediate proximity to the station number 3 with the closest lidar strobe being no farther than 2 m from the station. Two other stations were used to estimate the gradient Richardson's number and turbulent heat flows at the corresponding altitudes.
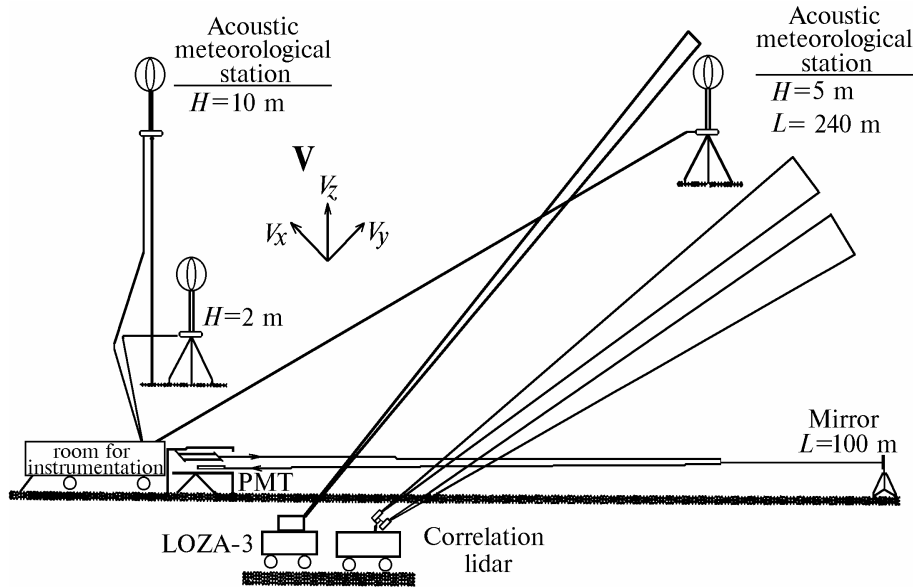
FIG. 1. Scheme of the laser—acoustic experiment to study atmospheric aerosol.

In the course of the experiment 50 measurements have been carried out each of 17 min continuous record. The number of points in a series was 2048. The discretization frequency in a recording was 2 Hz. Total number of degrees of freedom in estimation of the spectra approached 30. They ensured no worse than 18% accuracy of autospectrum estimates.

The synchronous measurements have allowed us to calculate various auto— and cross—correlations as well as auto— and cross—spectra. Now we present several plots of measurement series No. 10 made on July 27, 1993 at 12:00 of local time.[12] Figure 2 shows the autocorrelation of lidar signal and the cross—correlation function of the same signal with tangent component of wind velocity. Figure 3 shows autospectra of tangent velocity and lidar signal, together with their functions of coherence and phase. From the figures we see that the frequency spectrum contains section with a 5/3 slope in accordance with Kolmogorov—Obukhov power law.
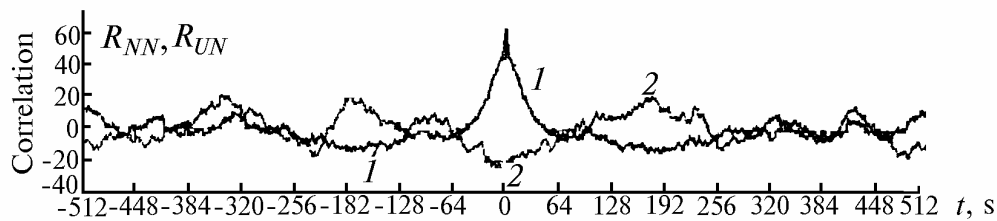
FIG. 2. Autocorrelation function of lidar signal (1) and cross—correlation function of the same signal with tangent wind velocity component (2), both normalized to the variance and multiplied by 100.
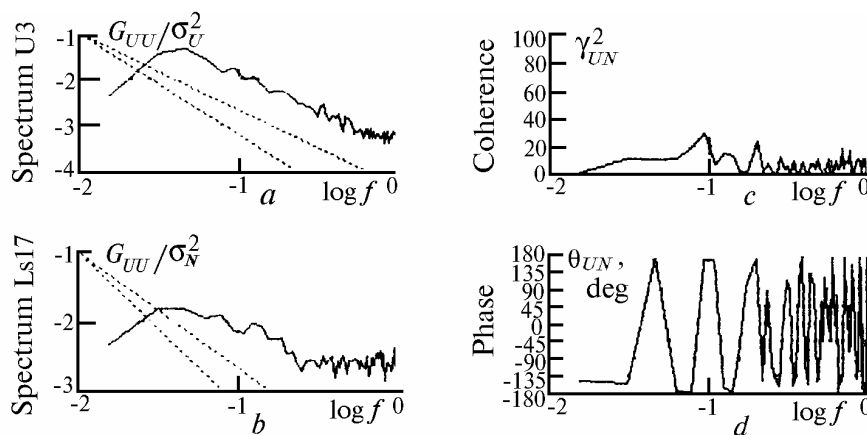
FIG. 3. Normalized autospectra of tangent wind velocity (a) and lidar signal (b), and the functions of coherence (c) and phase (d).

From Figures 2 and 3 it is obvious that the aerosol concentration fluctuates out of phase with the oscillations of tangent component of wind velocity. This causes the presence of negative correlations and phase differences of up to 180°. Nevertheless, the coherence spectrum is well within 0.3, thus indicating the complicated (nonlinear) relation between the wind velocity and aerosol fields.

Figure 4 shows co–spectra (the real parts of cross–spectra) of horizontal and vertical flows of heat and aerosol as obtained in the near–ground atmospheric layer on July 27, 1993 at 11 a.m. for cloud cover index of 7–8 and unstable temperature stratification (Richardson number Ri = − 0.07).[13] Clearly, the figure confirms the fact that the ratio of horizontal to vertical heat flow in the near–ground layer is negative (for any stratification), like the ratio of air flows themselves. From the figure it follows that from 60 to 90% flows is carried by inhomogeneities corresponding to the frequency lower than 0.1 Hz (or in extent of over 30–50 m). The wind speed at the altitude of 5 m (station 3) was 2.4 m/s, the horizontal and vertical heat flows were 148 and 33 J·m^{-2}·s^{-1}, and the corresponding particle flows normalized to variance were 0.174 and 0.122 m^{-2}·s^{-1}.

These experimental results clearly indicate the existence of close relation between the lidar characteristics of aerosol fields and the atmospheric turbulence, a convincing reason for subsequent use of laser sensing data alone to treat atmospheric turbulence.

Distinct anisotropy of fluctuation characteristics of velocity, temperature, and, hence, particle flows in horizontal and vertical directions should be mentioned here as a specific feature. This reinforces the need in an adequate theoretical description of lidar signal fluctuations in an anisotropic field of aerosol

inhomogeneities. We have developed such a description[14] presented below.
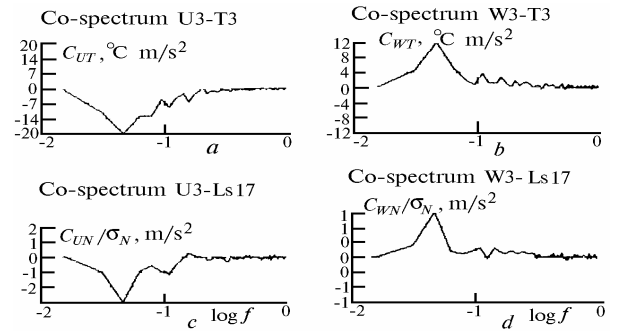

FIG. 4. Co–spectra of horizontal heat flows (a) and aerosol content (c), and the corresponding vertical flows of these quantities (b and d).

We assume that the components V_x, V_y, and V_z of wind velocity have normal distribution with the mean V_0 and the variances σ^2, and that the spectrum of spatial fluctuations of aerosol particle concentration is of the form

$$\Phi_N(\kappa) = 0.033\, C_N^2\, \kappa^{-11/3}\, (1 - \exp(- \kappa^2/\kappa_0^2))\, ,$$

where $k_0 = 2\pi/L_0$, L_0 is the outer scale of turbulence, and C_N^2 is the structure characteristic of concentration fluctuations. Then, in accordance with Ref. 8, the normalized spatiotemporal correlation function of backscattered radiation is

$$\frac{R(\mathbf{r},\,t)}{R(0,\,0)} = B^{-1}\left\{\left(a_V^2 + \kappa_0^{-2} + \tfrac{1}{2}\sigma^2\tau^2\right)^{1/3}{}_1F_1\left[-\tfrac{1}{3};\tfrac{3}{2};\frac{-(\mathbf{r}-\mathbf{V}_0\tau)^2}{4\left(a_V^2 + \kappa_0^{-2} + \tfrac{1}{2}\sigma^2\tau^2\right)}\right] - \left(a_V^2 + \tfrac{1}{2}\sigma^2\tau^2\right)^{1/3}{}_1F_1\left[-\tfrac{1}{3};\tfrac{3}{2};\frac{(\mathbf{r}-\mathbf{V}_0\tau)^2}{4\left(a_V^2 + \tfrac{1}{2}\sigma^2\tau^2\right)}\right]\right\},\ (1)$$

where $B = \left(a_V^2 + k_0^{-2}\right)^{1/3} - a_V^{2/3}$, a_V are the extents of scattering volumes, r is their spacing, τ is the time delay, and ${}_1F_1(a,\,b,\,x)$ is the hypergeometric function. The above expression is obtained assuming equality of variances of wind velocity components. The common practice, however,

is the presence of anisotropy in wind velocity fluctuations. To evaluate this factor, we analytically calculated $R(2,\,\tau)/R(0,\,0)$ for the case when the vertical fluctuations of wind velocity are different from the horizontal ones $(\sigma_x = \sigma_y = \sigma \neq \sigma_z)$. Resulting expression is

$$\frac{R(\mathbf{r},\,t)}{R(0,\,0)} = B^{-1}\left\{\frac{\left(a_V^2 + \kappa_0^{-2} + \tfrac{1}{2}\sigma^2\tau^2\right)^{5/6}}{\left(a_V^2 + \kappa_0^{-2} + \tfrac{1}{2}\sigma_z^2\tau^2\right)^{1/2}}\Theta_1\left[\tfrac{1}{2},-\tfrac{1}{3},\tfrac{11}{6};\tfrac{3}{2};\frac{-\tfrac{1}{2}(\sigma^2-\sigma_z^2)\tau^2}{a_V^2+\kappa_0^{-2}+\tfrac{1}{2}\sigma_z^2\tau^2},\frac{-(\mathbf{r}-\mathbf{V}_0\tau)^2}{4\left(a_V^2+\kappa_0^{-2}+\tfrac{1}{2}\sigma^2\tau^2\right)}\right] - \right.$$

$$\left. - \frac{\left(a_V^2 + \tfrac{1}{2}\sigma^2\tau^2\right)^{5/6}}{\left(a_V^2 + \tfrac{1}{2}\sigma_z^2\tau^2\right)^{1/2}}\Theta_1\left[\tfrac{1}{2},-\tfrac{1}{3},\tfrac{11}{6};\tfrac{3}{2};\frac{-\tfrac{1}{2}(\sigma^2-\sigma_z^2)\tau^2}{a_V^2+\tfrac{1}{2}\sigma_z^2\tau^2},\frac{-(\mathbf{r}-\mathbf{V}_0\tau)^2}{4\left(a_V^2+\tfrac{1}{2}\sigma^2\tau^2\right)}\right]\right\},\ (2)$$

where $\Theta_1(a,\,a',\,b;\,c;\,t,\,x)$ is the hypergeometric function of two variables. Note, if in Eq. (2) we take $\sigma_z = \sigma$, then $t = 0$, $\Theta_1(a,\,a',\,b;\,c;\,0,\,x) = {}_1F_1(a',\,c,\,x)$, and the formula (2) reduces to formula (1).

Figure 5 shows the ratio $R(\mathbf{r},\,\tau)/R(0,\,0)$ for $\sigma_z = 0$ and $\sigma_z = \sigma$, as calculated by Eq. (2) for $a_V = 1$ m, $L_0 = 80$ m, $r = 5$ m, and $V_0 = 1$ m/s. As is seen, the

effect of anisotropy of wind velocity fluctuations on correlation function is as follows: decreasing the variance σ_z^2 of the vertical wind component below the horizontal one σ^2 shifts the correlation peak toward larger τ values, broadens the correlation function, and increases the maximum correlation over the level of isotropic fluctuations.
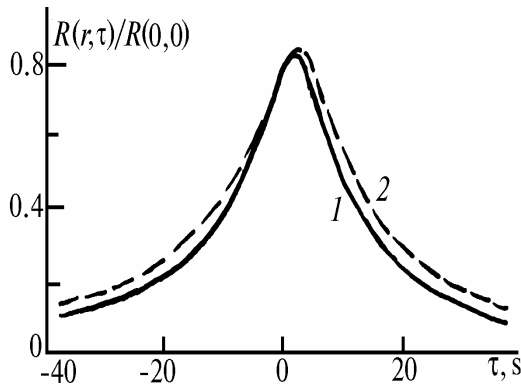
FIG. 5. The influence of anisotropy of wind velocity on cross–correlation function of lidar signal: $\sigma_x = \sigma_y = \sigma_z = \sigma$ (1) and $\sigma_x = \sigma_y = \sigma$, $\sigma_z = 0$ (2).

An alternative way of processing lidar signals is the use of coherent analysis methods. In Ref. 8 the effect of wind velocity fluctuations on spectral characteristics of lidar signals was evaluated for the case of $\sigma^2/V^2 \ll 1$. However, there can occur meteorological situations where σ^2/V_0^2 approaches or exceeds unity. The account for wind fluctuations at arbitrary σ^2/V_0^2, for the cross–spectrum $W(\mathbf{r}, \omega) = \dfrac{1}{2\pi} \int\limits_{-\infty}^{+\infty} R(\mathbf{r}, \tau)\, e^{-i\omega\tau}\, d\tau$ we obtain

$$W(\mathbf{r}, \omega) = c\, \frac{1}{V_0} \exp\left(-\frac{i\omega r}{V_0}\right) \int\limits_0^\infty \kappa\, \Phi_N(\kappa) \times$$

$$\times \exp\left(-a_V^2\, k^2 - \frac{\sigma^2\, r^2\, k^2}{2\, V_0^2}\right) \left\{ \mathrm{erf}\left(\frac{V_0}{\sqrt{2}\,\sigma} - \frac{\omega}{\sqrt{2}\,k} + i\,\frac{\sigma\, r\, \kappa}{\sqrt{2}V_0}\right) + \right.$$

$$\left. + \mathrm{erf}\left(\frac{V_0}{\sqrt{2}\,\sigma} + \frac{\omega}{\sqrt{2}\,\kappa} - i\,\frac{\sigma\, r\, \kappa}{\sqrt{2}V_0}\right)\right\}\, d\kappa\,, \tag{3}$$

where $\omega = 2\pi f$, and f is the frequency. (For simplicity, the spacing $\mathbf{r}$ of scattering volumes is assumed to be oriented in the same direction as $\mathbf{V}_0$, with $\sigma_x = \sigma_y = \sigma_z = \sigma$).

The behavior of the coherence spectrum $\gamma(\mathbf{r}, \omega) = |W(\mathbf{r}, \omega)|/|W(0, 0)|$ and the phase spectrum $\Theta(\mathbf{r}, \omega) = \arctan \mathrm{Im}\, W/\mathrm{Re}\, W$ is illustrated in Fig. 6. The theoretical curves presented are calculated by numerical integration of Eq. (3) for $a_V = 0.2$ m, $L_0 = 80$ m, and $r = 5$ m. Curves 1–3 describe the decrease of $\gamma^2(\mathbf{r}, \omega)$ due to wind velocity fluctuations. The low–frequency portion of coherence spectrum saturates, with values depending on $\sigma_V^2 = 3\sigma^2$, before vanishing at high frequencies. We note, that in the case of no wind fluctuations, the coherence spectrum is frequency independent with a unit value, while the phase spectrum behaves linearly (see curves 4' and 5'). The presence of wind fluctuations increases the slope of phase spectrum by an amount proportional to σ_V (see curves 1'–3'). It is important that for large ratios σ_V/V_0 (curve 2) $\Theta(\mathbf{r}, \omega)$ behaves essentially nonlinearly.
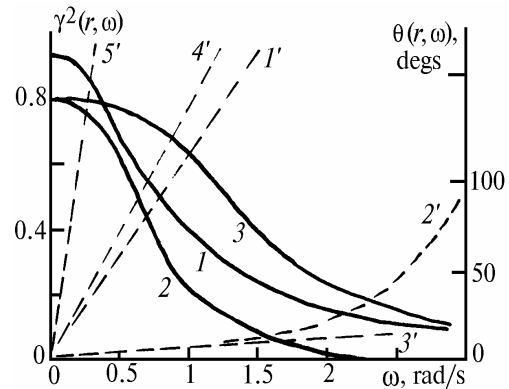

FIG. 6. The behavior of coherence and phase spectra in the presence of intense wind velocity fluctuations (theoretical calculation): coherence spectrum (1–3) and phase spectrum (1'–5'); for $V_0 = 2$ m/s: $\sigma_0/V_0 = 0$ (4'), 0.5 (1 and 1'), and 5 (3 and 3'); and for $V_0 = 0.5$ m/s: $\sigma_0/V_0 = 0$ (5') and 10 (2 and 2').

The theoretical calculations were verified by field experiments using two–path lidar[15] and three–component ultrasonic anemometer,[16] the latter was used to measure mean values and pulsations of wind velocity. The laser beams were directed to the atmosphere along a horizontal path with the angular separation of 3.5°; the resulting time series were then processed using correlation method. Figure 7 presents the calculated and experimental correlation functions obtained for $r = 7.5$ m, $\sigma_x = \sigma_y = 0.22$ m/s, $\sigma_z = 0.077$ m/s, and $V_0 = 1.41$ m/s. Curves in the figure show quite a reasonable agreement of the correlation functions, both in shape and values. This fact validates the description just developed and shows once more the need for the account for strong wind velocity fluctuations and their anisotropy when interpreting data of incoherent laser sensing of aerosol atmosphere. In doing so, Eqs. (2) and (3) can be regarded as a basis for laser methods of remote monitoring of atmospheric turbulence.
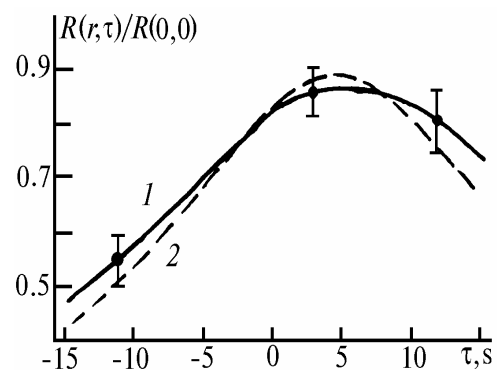

FIG. 7. The experimental (1) and theoretical (2) correlation functions of returns at 2.5 m altitude. Vertical bars show rms deviations.

LIDAR MONITORING OF AEROSOL POLLUTION IN THE ATMOSPHERE OVER A CITY

Lidar has proven itself an efficient tool for monitoring air pollution just after it had been created.[17] Subsequent

advances of air pollution control with lidars are summarized in Ref. 18. Attractive factor here is the possibility of independent (unapproved) remote and quantitative monitoring of industrial emissions, their diffusion, and spatial distribution over areas of some tens of square kilometers. Recently, observational methods have been modified, the details of the pollution emission intensity estimation have been ascertained, and the unique data of long–term observations of an individual pollution plume have been accumulated. These results will be considered below in a more detail.

In laser sensing the information about aerosol concentration is obtained from lidar signal or its range squared analogue, S–function.[19] By inverting equation of laser sensing, which contains the experimental S–function (details of the inversion can be found in Ref. 19), we obtain the profile along the sounding path or, as in scanning, the corresponding transection of scattering or extinction coefficient of the atmosphere for laser radiation, that is, in either case an intermediate optical characteristic is to be inverted into the mass concentration of aerosol (mg·m^{-3}). Relations of the extinction coefficient − concentration type are determined by a complicated dependence on particle composition, shape, and size–distribution. Reference 18 explores theoretically and experimentally the coupling coefficient μ between these characteristics and shows that in practical cases it may widely vary, $\mu = (0.52 \pm 0.34)$ mg·km·m^{-3}. This circumstance is likely to be mostly due to the specific features of aerosol, because of its microoptical and microphysical characteristics.[1] Nevertheless, on the base of the analysis of studies of different

industrial smokes, the review in Ref. 19 shows close correlation between the optical density of a source of pollution and the concentration of pollutants in it. Moreover, for smoke of some types the coefficient μ is almost independent of meteorological conditions. This occurs for smokes in which the mean radius of aerosol particles fits the Mie parameter, $1 < \rho < 3$–6 as well as for smokes containing weakly hygroscopic particles. This emphasizes the necessity of preliminary empirical studies or, at least, a classification of aerosol depending on the source of pollution; this should be done in all districts, in order to reduce the error in evaluation of mass concentration from lidar measurements. For pollution sources of Kemerovo, Tomsk, and Pavlodar such relations were obtained and were really helpful in quantitative mapping of the atmospheres over those cities.

Figure 8 illustrates the application of the aerosol scanning lidar LOZA−3 (Refs. 11 and 19) to mapping of the distribution of optical–physical parameters (scattering coefficient − mass concentration) of aerosol fields over Kemerovo city, whose layout, including the river Tom', is shown by dashed lines. On the transection, the aerosol concentration is given as a degree of blackness, with scale shown on the lower portion of the figure. This draw is rather semiquantitative presentation of an actual distribution of aerosol concentration. Nevertheless, these data present a numerical array, stored in a computer; so it is always possible to extract the qualitative information for any point on the map with the spatial resolution 3 to10 m, characteristic of a given lidar.
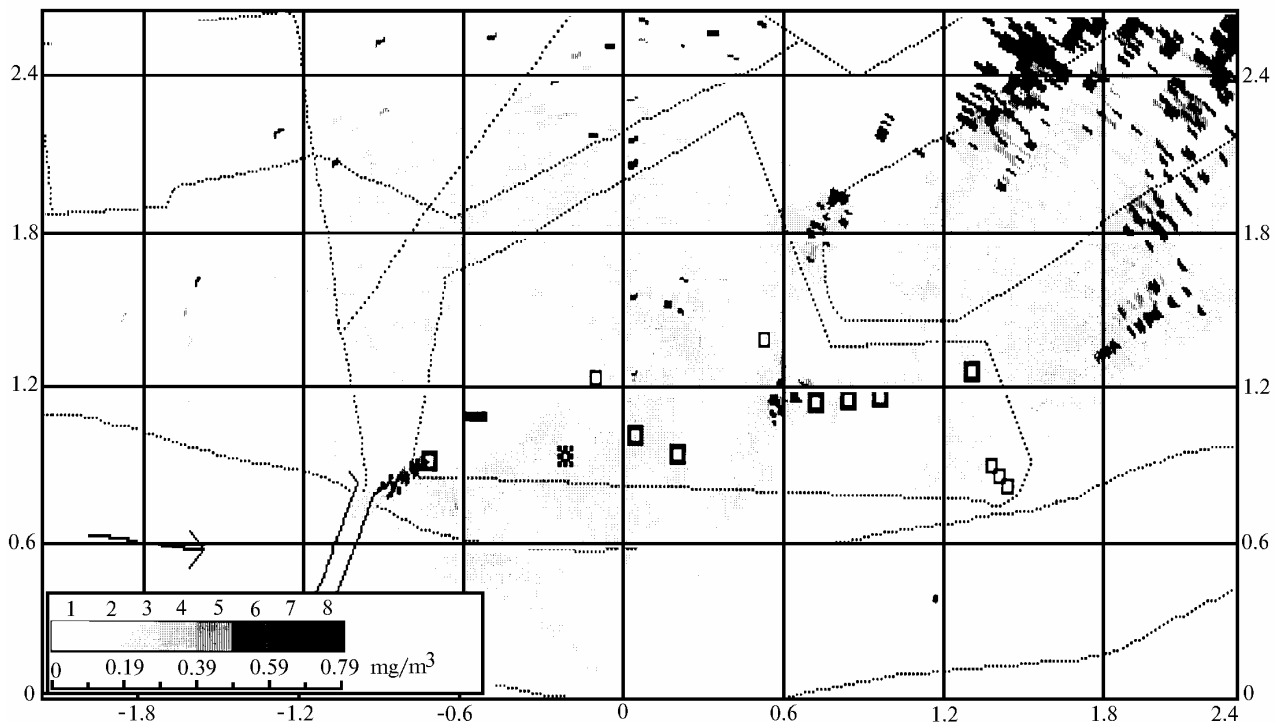

FIG. 8. Mapping of aerosol pollution distribution in azimuth scanning at angle of 10° at Kemerovo. The location of lidar is marked as 0 on the ordinate.

In addition to the estimation of mass concentration of aerosol pollutants, the lidar is also capable of determining the pollution rate (in g/s) of local sources (such as boilers, thermal and electric power stations, and plants). This can be made by direct sensing of smoke plumes to yield total

horizontal or vertical section. For definiteness, we shall restrict ourselves to scanning over a vertical plane.

Following simple argumentation, one can readily arrive at the estimation of the pollution rate B (in g/s) as

$$B = V\mu \cos\varphi \int_S \alpha(S')\,\mathrm{d}S' \;,$$

where V is the aerosol transport velocity in the smoke plume, S is the plume vertical section, $\alpha(S)$ is two-dimensional distribution function of scattering coefficient over the plane S.

As it stands, the angle φ takes into account the fact that the sensing direction and the direction of plume propagation are not strictly perpendicular. It can readily be obtained from horizontal sections, because all sensing directions can be fixed in the absolute angular coordinate system. Also, transport velocity can be measured by the same lidar by tracking the transport of aerosol inhomogeneities and using correlation or spectral processing of time and/or spatial series of lidar returns.[20] The measurements of atmospheric flows velocity will be discussed in the next section in detail.

Another important problem in the pollution intensity estimation is to choose correctly the position of lidar section in the smoke plume, under the guidance of the lidar technical characteristics and some specific features of the method employed.

Generally, most technological processes release into the atmosphere a lot of water vapor, in addition to the solids. This may lead to many local supersaturations and, thus, to thicker water—coated aerosol particles.

As theoretical calculations show,[21] relative humidity on the axis of a smoke plume has minimum value near stack mouth and a maximum at a distance of 300—400 m from it, depending on the meteorological conditions and the cloud parameters. The zone of moist soot particles extends to approximately 1000 m.

The calculations clearly indicate that the sounding is preferred either just above the stack mouth or in the far zone of a smoke plume. However, small geometric size of smoke plume near stack mouth may appear well beyond the angular and spatial resolution of a lidar.

Sounding in the far zone may be problematic too. Very often plume at such separations is no longer integral, but is broken into pieces by the atmospheric turbulence. In addition, in the presence of several sources of pollution it is highly probable that smoke plumes at large distance will merge together to give a common aerosol field.

Thus, it is clear that there is certain distance from the pollution source, optimal for taking a full cross section of a smoke cloud by scanning section. Analysis of theoretical and experimental results have shown the distance to be of the order of 50—100 m. This outcome is supported by Fig. 9 showing the dynamics of smoke from electric power station with 150 m high stack, located at the square with coordinates $x = -0.6$ and -1.2 and $y = 0.6$ and 1.2 (Fig. 8) (see Ref. 19).
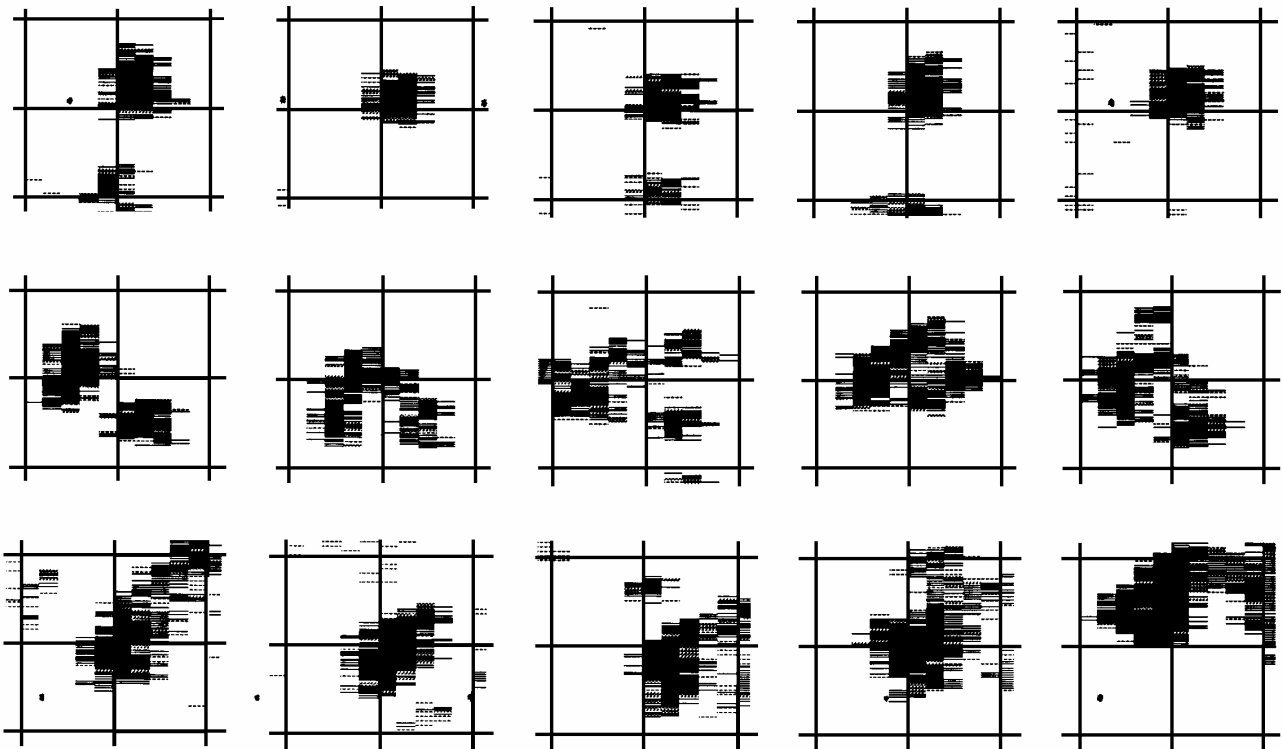

FIG. 9. *Vertical sections of electric—power—station smoke plume vs. time (time interval of* 2 min*) and distance from stack mouth of* 50 *(upper row),* 100 *(middle row), and* 150 m *(lower row). The size of map grid is* 75×75 m.

As is seen from the figure, when moving away from the source the plume, as expected, increases in thickness, although keeping its integrity in far zone (Fig. 5, middle and lower rows). However, the smoke in near zone is broken into two parts, normally equal in size. In our opinion, existence of the lower part of the cloud is due to the sedimentation of large—sized soot particles, starting just near the stack mouth. The absence of such pattern in subsequent cycles (Fig. 9, middle and lower rows) indicates that the sedimentation zone ends at 100 m.

This also favors the use of near—source cloud cross sections in pollution rate estimation.

The behavior of smoke may be of independent interest from the viewpoint of long—range transport of pollutants,

with their impact extended to adjacent territories. For studies of long–range transport, airborne lidars are more promising. For instance, the aircraft–laboratory AN–30 Optik–E,[22] equipped with aerosol lidar Makrel–2M,[23] has been used at the Institute of Atmospheric Optics for several years.

Of the set of data available, we select three typical ones, which most clearly demonstrate the lidar capabilities in dynamical treatments and could not be obtained by other instrumentation. Figure 10 shows the transformation of smoke plume, produced by Amursk industry (Khabarovsk region), on its way toward Komsomol'sk–na–Amure. Here the upper portion of the figure demonstrates the sounding scheme: section (a) is made windward of Amursk at a distance of 2 km

from the pollution source ($x = -2$ km), section (b) at a distance of 2 km leeward of the source ($x = +2$ km), and section (c) at a distance 22 km from source ($x = +22$ km) in Komsomol'sk–na–Amure suburb. All of the transections were accomplished in the direction normal to wind direction at the flight altitude of 250 m. According to the data of thermodynamical complex onboard the aerocraft–laboratory, the temperature inversion occurred at an altitude of 190 m. Wind velocity and direction were determined by airborne navigation system directly during flight. In all figures, the unitary isogramms were taken to be the values of backscattered signals corresponding to the mass concentration of $M = 0.01$ mg·m^{-3}.
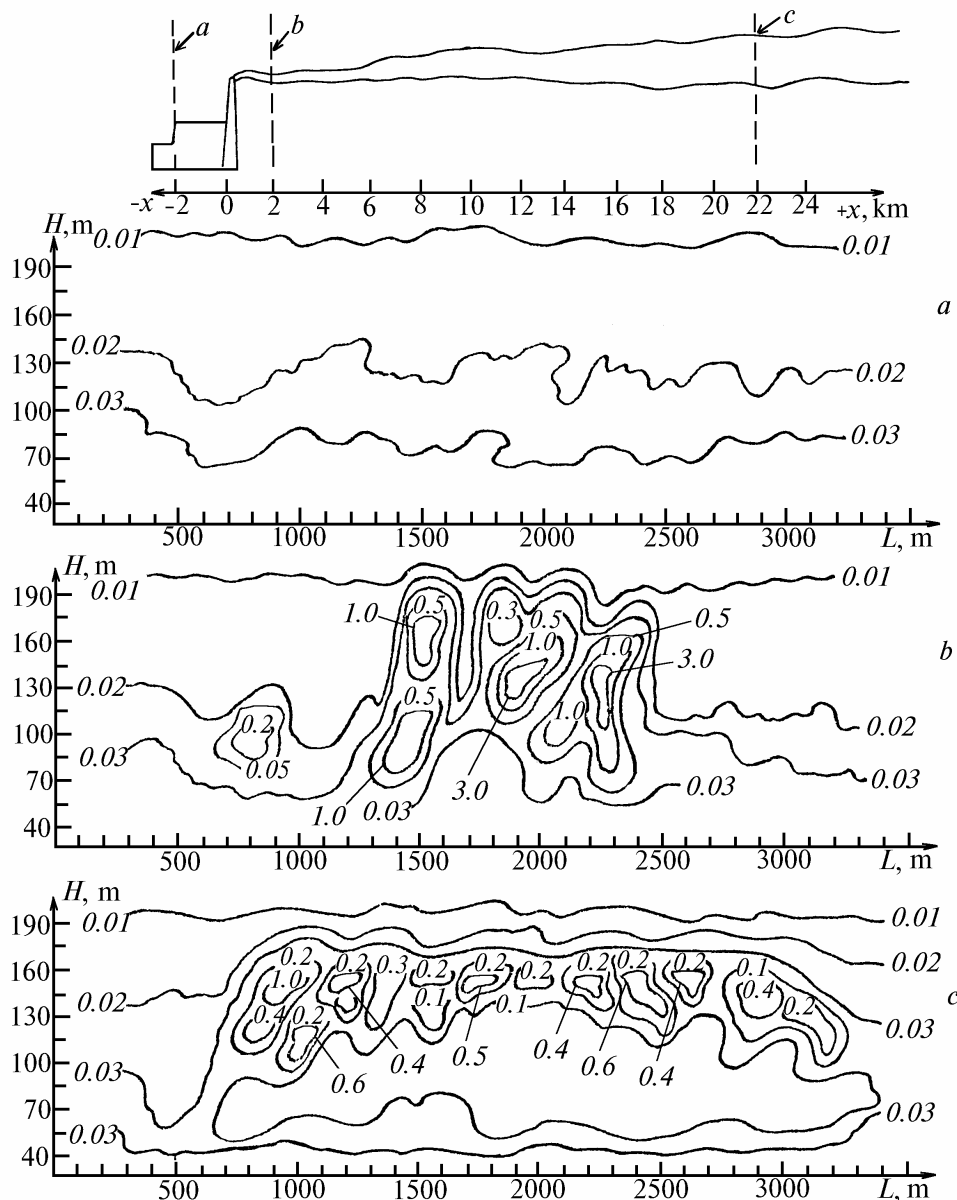

FIG. 10 The vertical distribution of mass concentration (in relative units) of aerosol near Amursk, observed on December 18, 1990: windward side (a), 2 km away from stacks (b), and 22 km away from stacks (c); uppermost section shows the scheme of experiment.

Figure 10*a* indicates that the air arriving at Amursk is clear. Although, below the inversion layer there is somewhat increased aerosol concentration, caused by natural processes. Behavior of isogramms in this layer is governed by the underlying surface, whose influence is restricted to sub—inversion altitudes (the curve near 200 m is more monotonic). There are no pollution sources on this side of the town.

As Fig. 10*b* shows, the smoke plume leaving Amursk remain fairly compact up to 2 km away from town and includes almost all emissions. It is restricted to the layer between 55 and 190 m and is 1200 m wide. At the same time, the mass concentration field inside the smoke plume is resolved into several separate streams with different densities (Fig. 10). Its upper boundary lies in the inversion layer (190 m). The layers above the inversion, on the unitary isogram, are perfectly unperturbed, that is the smokes so separated from the source have nearly ambient temperature. From Fig. 10*b* one can see the secondary, less powerful source, located at the altitude of 100 m. Below 50 m no sources of suspended particles around Amursk is observed.

The transection (Fig. 10*c*) by plane normal to the direction of transport at that altitude demonstrates the changes occurred inside the plume after it has traversed 20 km. Also, this transection characterizes the air entering Komsomol'sk—na—Amure through its south periphery. From Fig. 10*c* one can see that the cloud has doubled in width and became 2500 m wide in horizontal plane. At the same time, in the vertical plane its thickness decreased to 80—160 m. This is the result of balancing between plume and inversion layer, the former tending to "emerge" and the latter inhibiting the emergence. Finally, despite rather a long travel from Amursk to Komsomol'sk—na—Amure (about 32 min at the wind velocity of 12 m/s), it has preserved streaming shape typical of the original plume. Aerosol concentration inside the cloud has decreased three—fold, due presumably to its expansion. The cloud from the secondary source, apparent on the transection of Fig. 10*b*, is not detected at this distance. This is most probably because it has merged with the primary plume.

Of note in Fig. 10*c* is the extended, relatively homogeneous region with concentration outlined by isogram *10*, below which isogram *3* lies. Occurence of increased aerosol content below the cloud indicates the rapid growth of particles due to coagulation and condensation, thus stimulating their gravitational sinking. This "pouring out" occurs between 130 and 45 m. It seems that the sinking particles reach the surface with the lower flow but this depletion is effectively masked by pollution contribution of industry of Komsomol'sk—na—Amure.

The above outline of work on ecological monitoring of industrial conglomerates clearly illustrates the capabilities of remote lidar methods, in contrast to other techniques.

THE APPLICATION OF AEROSOL LIDAR TO DETERMINATION OF PROFILE OF WIND VELOCITY

Knowledge of wind characteristics seems to be important for many applications such as weather forecast, transport of pollutions, flights of objects in the atmosphere.

In this connection, development of a lidar technique to measure wind velocity is very important. The Doppler approach to laser measurements of wind velocity requires high—quality lidars. These difficulties are avoided using an alternative approach: correlation method.

The correlation methods deal with natural inhomogeneity of atmospheric optical parameters (mainly of aerosol nature) and are based on the analysis of fluctuating lidar signals as reflected by several spatially—separated scattering volumes at each altitude of interest. Time required for atmospheric

inhomogeneities to travel between two volumes sounded is a measure of the corresponding wind velocity component.

Optical investigations of inhomogeneities of the atmospheric scattering properties, employing ground and airborne lidar facilities, have proved the existence of inhomogeneities of scattering coefficient, justifying the application of correlation methods, at least for the lowermost, 5—km layer, as well as the tropo— and mesopause altitudes.

The use of the correlation method for wind velocity measurements suggests employing at least three sounding paths for data acquisition. Technically, this is done using either three—beam lidars or scanning lidars.[20] Recently, correlation lidars for wind velocity profile measurements have been developed in Russia, Bulgaria, USA, and Netherlands, with the operational altitude range of 1—3 km. Measurement time per one profile is 5—10 min. Spatial resolution may widely vary: from 3 to 100 m in vertical, and from 30 to 500 m in horizontal plane.

An extension of correlation methods to other applications may proceed as the corresponding change in data acquisition, to give either values of wind velocity along a given direction or over a given area, or an average value over the line or the area. Moreover, incorporation of spectral analysis in algorithms of laser return processing can make it possible to estimate such characteristics of turbulence as turbulence strength and kinetic energy dissipation rate. This last outcome allows the application of correlation lidars to monitoring of dynamics of the atmospheric boundary layer.

For a detailed characterization of the correlation method, having been developed at the Institute of Atmospheric Optics for over 15 years, see Refs. 20 and 24.
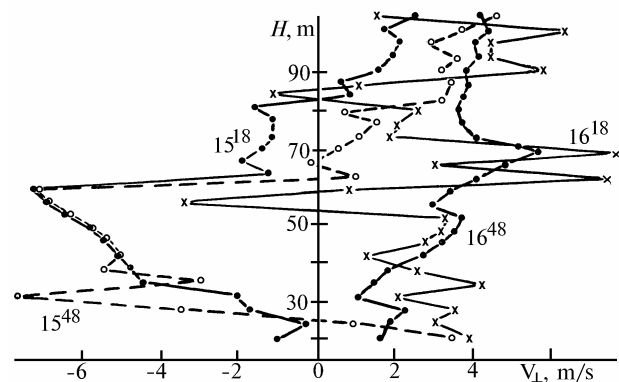

FIG. 11. Vertical wind profiles as obtained by correlation lidar when sensing along slightly inclined path over city. Numbers near curves indicate local time of measurement. Right—hand side profiles refer to wind directions from 0 to 180° and left—hand side corresponds to directions from 180 to 360°.

As an illustration of capabilities of correlation methods, we present (Fig. 11) a particular result from sensing instantaneous (measurement time is 3 s) wind velocity; this is obtained in Sankt—Petersburg using small measurement base lidar with high pulse repetition frequency (50 Hz).[25] The lidar spatial resolution was 2—3 m. We notice that the standard radiosonde method of wind velocity profile measurement has at least one order of magnitude poorer resolution than data shown in the figure.

It is seen that wind velocity and direction in the near—ground layer over rough surface, experience strong variations, in both space and time.

Testing of correlation lidar under the conditions of precipitation in the atmosphere have demonstrated a degraded wind lidar performance, due to poor drop transportability, aerosol washing out, and the presence of large vertical component of droplet velocity. Nevertheless, measurements in light rain (with rate less than 2 mm·h^{-1}) are even easier to perform, than in the clear atmosphere, due to stronger signal compared to noise.

Analysis of returns from rain—drops has shown that the more efficient sensing was the result of increased fluctuating signal component. Limitations on wind measurements in rain can be expressed in terms of modal drop radius: it is larger for heavier rain, and smaller for lighter rain; so, for light rain with drop diameters less than 0.2 mm (Ref. 26) the transport velocity due to rain is 7—10 times greater than sinking velocity due to gravity, hence, such particles can be used as wind tracer.

In the month of August 1993, we carried out experimental studies of wind motion in light rainfall, typical of Siberia. Figure 12 presents profiles of wind velocity V and direction, as measured on August 25, 1993 under conditions of light cloudiness and drizzle.[27] As an independent check of wind measurements, we used theodolite to determine the velocity and direction (denoted by asterisk in the figure) of cloud motion from intersections of angular positions of inherent inhomogeneities at different instants of time. Values of cloud altitudes, necessary for theodolite calculations, were provided by lidar with high accuracy. As is clear from the figure, data from different methods agree well, further supporting the possibility of lidar measurements in light rainfall. Also, the lidar operational altitude range has increased to a value of approximately 2 km.
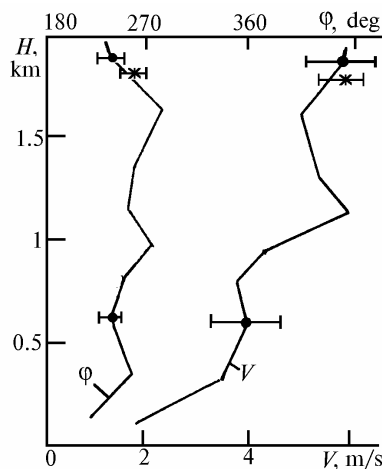

FIG. 12. The profiles of wind velocity and direction in drizzle, as measured by three—path lidar. The horizontal bars show the confidence interval at a probability of 0.95.

Recalling that the drop sinking velocity and drop size are related (through, e.g., the empirical curve of Hann and Cinzer[26]), one can use the correlation lidar to estimate drop size. Such estimation relies heavily upon the determination of upward droplet velocity. For details of determination of droplet sinking velocity in precipitations, see Ref. 27.

Undoubtedly, the possibility of obtaining such results using correlation method shows that further development of the correlation method is needed; moreover, it is much cheaper than Doppler method.

LASER SENSING OF AEROSOL ATMOSPHERE FROM SPACE

New facilities in atmospheric research, afforded by spaceborne lidars, has motivated recently the development of a number of spaceborne lidars, some of which have received wide application. In particular, Russian lidar Balkan—1 (Ref. 5) has been prepared for start aboard the modulus Spectr of Mir space station, while the Russian—French lidar Alisa is planned to be installed on the modulus Priroda of the same station.[28] NASA LITE satellite lidar experiment was carried out from 10 to 19 September 1994 on board Shuttle spacecraft.[29,30] Despite they included many simulated estimations, first satellite lidar measurements were more of technological (testing) rather than observational importance. This was called for by the need in actual data to refine lidar methods and their validation. Serious problems could appear in interpretation of lidar signals, as reflected by dense aerosol layers and clouds with substantial spatial inhomogeneity.

Well some problems of satellite laser sensing of aerosols and clouds can already now be approached using analysis of signals from geodetic laser range finders, which, in contrast to lidars, have been used in space several times (see, e.g., Ref. 31). The satellite laser range finders are intended to detect surface—reflected pulses from satellite at several hundred kilometers altitude, and in the case of laser beam striking the cloud they would record the corresponding returns. In this sense they are somewhat similar to lidar signals. At the Institute of Atmospheric Optics the processing was made of signals of satellite laser altimeters. Below we discuss the results of processing returns from clouds, as recorded by Russian satellite range finders of LORA type for period from 1982 to 1983 (see Ref. 32).

The range finder had transceiving devices with the following specifications:

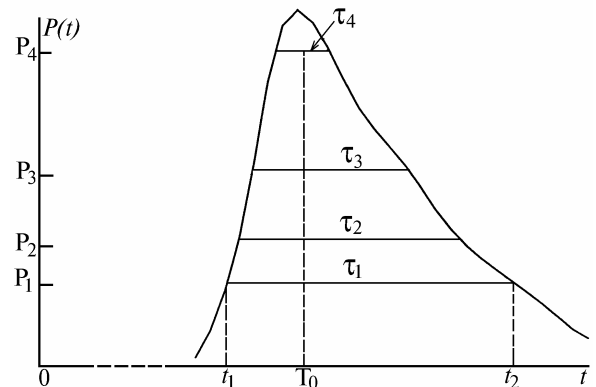|	
wavelength, nm	532
energy per pulse, J	0.15
pulse duration, ns	10
diameter of receiving telescope, m	0.27
angular beam divergence, sec. of arc	30
field—of—view angle, sec. of arc	60
sounding pulse repetition frequency, Hz	0.2

FIG. 13. The diagram of return record by a satellite laser range finder with four threshold layers.

According to the problem solved, the recording system of a range finder operates based on threshold

principle (Fig. 13). Four meters of time intervals (MTI) were used, switched on at different threshold powers level $P_1 \ldots P_4$. The lower level corresponds to light power $P_1 = 1.7 \cdot 10^{-8}$ W incident on the range finder receiving aperture, while the upper level to $P_4 = 1.1 \cdot 10^{-7}$ W. General time counting started with pulse sending. The first MTI switched on at moment t_1, when the value of received power $P(t)$ reached the level P_1, and switched off at t_2, thus giving the threshold duration $\tau_1 = t_2 - t_1$. The threshold durations $\tau_2 \ldots \tau_4$ were evaluated in the same way. For the signal with maximum power $P_{max} > P_4$ all four threshold durations were recorded, while for $P_1 < P_{max} < P_2$ only one value, τ_1. The distance to reflecting object was determined from T_0, the time interval from sending sounding pulse to the center of the uppermost interval of all those recorded (i.e., to the middle of τ_4 interval for the case presented on Fig. 13). Occurence of a cloud or the underlying surface type was recorded by photograph from onboard the satellite.

We have considered a series of measurements (a set of soundings, with one pulse every 5 s) during which a transition occurred from sounding underlying surface (sea or ground) to sounding cloud, or *vice versa*. In this case, change of arrival time of return signal can be used for more reliable, than by photograph, identification of cloud and determination of cloud top altitude (CTA). The total of 56 cases were analyzed, with sounded CTA's from 0.6 to 5 km. In 28 cases the signal was recorded only at the first threshold level, and only in 5 cases at all of the four. In so doing, the duration at the first threshold level was in the range from 22 to 200 ns, that corresponded to the sounded cloud depth, $r_1 \approx c\tau_1/2$, of 3–30 m.

The threshold principle of signal recording, common in range measurements, differs from amplitude–temporal one, typical of lidars; so it has required special procedures of signal conversion. We chose to model lidar signal using a set of discrete threshold readings. Modeling started with a signal calculated for horizontally homogeneous cloud in the single scattering approximation. The relatively small duration of return signal justified the use of the single scattering approximation. Cloudiness was modeled with the simplest models, such as homogeneous over path cloud with specified or unknown value of lidar ratio and with power–law distribution of extinction coefficient α. Values of parameters were adjusted by least–square method to minimize the difference between actual and assumed values.

Estimates gave the reconstructed α in the range from 14 to 500 km^{-1} (very wide range). Figure 14 compares the accumulated probability of occurrence of α, as given by our calculation, with data[33] for different cloud types. Satisfactory agreement for dense cumuliform clouds validates the α estimation performed.

Values of the lidar ratio b, disagree with the model ones more stronger. For instance, though its average is 0.07, in 25% of cases $b > 0.1$, i.e., well above its physically grounded value for water clouds.[34] As a rule, it occurs for signals with large durations at the lower levels (100 ns and longer). In addition, with such signals it is difficult to minimize discrepancy in fitting parameters using model with a specified b.

We believe that such an overestimation of b is due to the appreciable discrepancy between the real cloud characteristics and the model ones. Most probably, the reasons are: 1) possible presence of patches of oriented ice plates occurring at cloud tops in signals; 2) the occurrence

of stepwise cloud edge within the laser spot (of 50 or 10 m diameter), with the vertical step size comparable to the spot diameter; and, 3) most significant: a contribution of multiple scattering to return signal. The optical radius of spot on cloud boundary primarily governs the contribution of multiple scattering to the signal. For $R_{opt} = 1$, $\alpha = 30$ km^{-1}, and, as results of Ref. 35 show, even $R_{opt} = 1.5$ causes the decrement of signal decaying to decrease by a factor of 2.6, due to an increase in time of multiple scattering contribution. In the case of our processing procedure the result is the underestimation of α and overestimation of b.
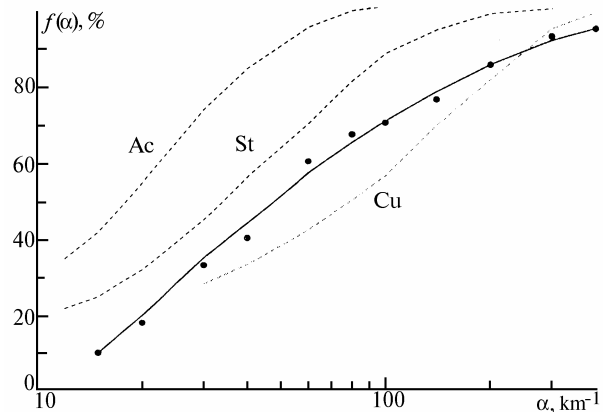

FIG. 14. The accumulated probability $f(\alpha)$ of occurence of the extinction coefficient in all soundings (solid curve) and the experimental data from Ref. 33 for different cloud types (dashed lines).

The results obtained do not contradict our understanding of cloud physics, so these can be regarded as a first experience of satellite laser sensing of the atmosphere. In addition, our estimates confirm the possibility of using spaceborne lidars to obtain physical information on cloud layers, and allow us to formulate more correctly the requirements to the instrumentation used. Of no doubt is also the necessity of further improvement of the mathematical methods of lidar signal processing, which take proper account of real broken cumulus cloud characteristics and multiple scattering. Moreover, we hope that with lidars of Balkan and LITE classes, having higher sensitivity and amplitude–temporal, not threshold, system of signal recording, we are able to attain a required depth into cloud and reconstruct cloud optical parameters with maximum possible accuracy. Use of lidars in space will cause the revolution in atmospheric research on global scale.

Summarizing the above discussion, we should like to note that the results presented do not restrict the capabilities of lidar methods for studying aerosol atmosphere. The use of the methods of differential absorption and scattering will provide grounds for remote monitoring of profiles of temperature and moisture, and thereby for creation of meteorological lidars. Implementation of coherent detection of returns, the basis of Doppler lidars, will make it possible to substantially increase the altitude range in laser sensing of atmospheric flows. Profound study of the relationship between spatiotemporal characteristics of lidar signals and atmospheric turbulence will aid a more detailed determination of profiles of atmospheric turbulence. So far little is known about the formation of aerosol fields under the impact of meteorological processes. Work in these and

other directions, toward further extension of the list of lidar−measured atmospheric parameters, is in progress.

ACKNOWLEDGEMENTS

REFERENCES

1. V.E. Zuev and V.V. Zuev, *Remote Optical Sensing of the Atmosphere* (Gidrometeoizdat, Leningrad, 1988), 232 p.

2. R. Measures, *Laser Remote Sensing* (John Willey and Sons, New York, 1987).

3. V.M. Orlov, I.V. Samokhvalov, and G.G. Matvienko, *Elements of Lightscattering Theory and Optical Location* (Nauka, Novosibirsk, 1982), 226 pp.

4. V.E.Zuev and I.E.Naats, *Inverse Problems of Laser Sensing of the Atmosphere* (Nauka, Novosibirsk, 1982), 241 pp.

5. Yu.S. Balin, V.V. Burkov, Znamenskii, et al., in: *Abstracts of Reports at 15th ILRC*, Tomsk (1990), pp. 12−14.

6. G.N. Baldenkov, E.E. Mozharov, M.N. Milenkii, et al., in: *Abstracts of Reports at 15th ILRC*, Tomsk (1990), pp. 380−381.

7. B.D. Belan, A.I. Grishin, G.G. Matvienko, and I.V. Samokhvalov, *Spatial Variability of Atmospheric Aerosol* (Nauka, Novosibirsk, 1989), 152 pp.

8. Yu.S. Balin, M.S. Belenkii, I.A. Razenkov, and N.V. Safonova, Opt. Atm. **1**, No. 8, 77−83 (1988).

9. I.A. Razenkov and A.P. Rostov, in: *Abstracts of Reports at the First Interrepublic Symposium on Atmospheric and Oceanic Optics*, Tomsk (1994), P. 2, pp. 99−100.

10. M.V. Anisimov, A.P. Rostov, G.Ya. Patrushev, et al., Prib. Tekh. Eksp., No. 4, 196−199 (1988).

11. Yu.S. Balin, G.S. Bairashin, and I.A. Razenkov, in: *Problem−Orientied Measurement−Calculational Complexes* (Nauka, Novosibirsk, 1989), pp. 65−71.

12. I.A. Razenkov, A.P. Rostov, and N.A. Shefer, in: *Abstracts of Reports at the First Interrepublic Symposium on Atmospheric and Oceanic Optics*, Tomsk (1994), P. 2, pp. 101−102.

13. I.A. Razenkov, A.P. Rostov, and N.A. Shefer, *ibid.*, pp. 103−104.

14. A.L. Afanas'ev, A.I. Grishin, G.G. Matvienko, et al., *ibid.*, pp. 40−41.

15. G.G. Matvienko, Opt. Atm. **1**, No. 6, 3−15 (1988).

16. A.P. Rostov, Atmos. Oceanic Opt. **6**, No. 1, 62−64 (1993).

17. R.T.H. Collis and E.E. Uthe, Opto−Electron. **4**, No. 2, 87 (1978).

18. V.E. Zuev, B.V. Kaul', I.V. Samokhvalov, et al., *Laser Sounding of Industrial Aerosols* (Nauka, Novosibirsk, 1986), 188 pp.

19. Yu.S. Balin and I.A. Razenkov, Atmos. Oceanic Opt. **6**, No. 2, 104−114 (1993).

20. G.G. Matvienko, G.O. Zadde, E.S. Ferdinandov, et al., *Correlation Methods for Laser−Location Measurements of Wind Velocity* (Nauka, Novosibirsk, 1985), 224 pp.

21. Yu.E. Geints and A.A. Zemlyanov, Atmos. Oceanic Opt. **5**, No. 5, 337−342 (1992).

22. *AN−30 Aircraft−Laboratory AN−30 Optik−E. Prospect*, Scientific Center of the Siberian Branch of the Russian Academy of Sciences, Tomsk (1990), 24 pp.

23. A.I. Abramochkin, I.E. Penner, and V.S. Shamanaev, Atm. Opt. **4**, No. 3, 262−263 (1991).

24. V.M. Orlov, G.G. Matvienko, I.V. Samokhvalov, et al. *Application of Correlation Methods to Atmospheric Optics* (Nauka, Novosibirsk, 1983), 160 pp.

25. G.G. Matvienko, I.V. Samokhvalov, V.S. Rybalko, et al., Opt. Atm. **1**, No. 2, 68−72 (1988).

26. A. Ishimaru, *Wave Propagation and Scattering in Random Inhomogeneous Media* [Russian translation] (Mir, Moscow, 1981), Vol. 1, 280 pp.

27. A.I. Grishin, A.E. Zilberman, and G.G. Matvienko, in: *Abstracts of Reports at the First Interrepublic Symposium on Atmospheric and Oceanic Optics, Tomsk* (1994), P. 2, pp. 38−39.

28. *International Purposeful Satellite Project "Nature". Scientific Measurement Program*, Institute of Radioelectronics of the Russian Academy of Sciences, Moscow (1991), 136 pp.

29. R.H. Coach, C.W. Rowland, K.S. Ellis, et al., Opt. Eng. **30**, No. 1, 88−95 (1991).

30. M.P. McCormic, D.M. Winter, E.V. Browell, et al., Bulletin American Meteorol. Soc. **74**, No. 2, 205−214 (1993).

31. J.L. Bafton, TIIER **77**, No. 3, 71−88 (1984).

32. G.P. Kokhanenko, G.G. Matvienko, V.S. Shamanaev, et al., Atmos. Oceanic Opt. **7**, No. 7, 517−521 (1994).

33. E.M. Feigelson, ed., *Radiation in Cloudy Atmosphere* (Gidrometeoizdat, Leningrad, 1981), 280 pp.

34. D. Deirmendjian, *Electromagnetic Scattering on Spherical Polydispersions* (American Elsevier, New York, 1969).

35. G.M. Krekov, M.M. Krekova, and I.V. Samokhvalov, Issled. Zemli iz Kosmosa, No. 2, 44−51 (1988).